

Abstract. This is an example SIAM L^AT_EX article. This can be used as a template for new articles. Abstracts must be able to stand alone and so cannot contain citations to the paper's references, equations, etc. An abstract must consist of a single paragraph and be concise. Because of online formatting, abstracts must appear as plain as possible. Any equations should be inline.

Key words. example, L^AT_EX

AMS subject classifications. 68Q25, 68R10, 68U05

1. Introduction. The introduction introduces the context and summarizes the manuscript. It is important to clearly state the contributions of this piece of work. The next two paragraphs are text filler, generated by the `lipsum` package.

Nam dui ligula, fringilla a, euismod sodales, sollicitudin vel, wisi. Morbi auctor lorem non justo. Nam lacus libero, pretium at, lobortis vitae, ultricies et, tellus. Donec aliquet, tortor sed accumsan bibendum, erat ligula aliquet magna, vitae ornare odio metus a mi. Morbi ac orci et nisl hendrerit mollis. Suspendisse ut massa. Cras nec ante. Pellentesque a nulla. Cum sociis natoque penatibus et magnis dis parturient montes, nascetur ridiculus mus. Aliquam tincidunt urna. Nulla ullamcorper vestibulum turpis. Pellentesque cursus luctus mauris.

Nulla malesuada porttitor diam. Donec felis erat, congue non, volutpat at, tincidunt tristique, libero. Vivamus viverra fermentum felis. Donec nonummy pellentesque ante. Phasellus adipiscing semper elit. Proin fermentum massa ac quam. Sed diam turpis, molestie vitae, placerat a, molestie nec, leo. Maecenas lacinia. Nam ipsum ligula, eleifend at, accumsan nec, suscipit a, ipsum. Morbi blandit ligula feugiat magna. Nunc eleifend consequat lorem. Sed lacinia nulla vitae enim. Pellentesque tincidunt purus vel magna. Integer non enim. Praesent euismod nunc eu purus. Donec bibendum quam in tellus. Nullam cursus pulvinar lectus. Donec et mi. Nam vulputate metus eu enim. Vestibulum pellentesque felis eu massa.

The paper is organized as follows. Our main results are in ??, our new algorithm is in ??, experimental results are in ??, and the conclusions follow in ??.

2. Related Work. One of the earliest work on parallelizing kernels having loop-carried dependencies is the red-black Gauss-Seidel scheme [8]. Later Kamath and Sameh introduced a two-block partitioning scheme for parallelizing Kaczmarz method on tridiagonal structures [14]. A general study on the convergence of these block methods were done by Elfving in 1980 [7].

The advent of processors having more parallelism and the need to consider more unstructured matrices have made graph-based approach an important tool for parallelizing such kernels. Multicoloring is one of the most popular approach used in this field [13], but is sometimes not efficient on modern cache-based processors. There have been several researches going on to increase the efficiency of multi-coloring and improving the heuristics, an overview of the methods can be found in [17]. One of the most successful method in this regard is the algebraic block multi-coloring [12] proposed by Iwashita et al. in 2012.

Another line of research focuses on parallelizing dependent kernels while maintaining the same convergence behavior of sequential execution. One of the earliest

*Submitted to the editors DATE.

Funding: This work was funded by the Fog Research Institute under contract no. FRI-454.

known works in this category is the hyperplane method [22] on FDM (Finite Difference Method) like matrices. Extensions to this approach can be seen in [19] where a hybrid approach between multi-coloring and hyperplane method is used. However the most general method which falls into this category is level-scheduling [22]. Efficient implementation of this method can be attributed to Park et al. with his work on triangular solvers [20].

Most of the above mentioned method have been tested only for their applicability to parallelize distance-1 dependent kernels and some of them are not capable to deal with dependencies like distance-2. The research on parallelizing distance-1 dependent kernels has been strongly accelerated after the introduction of HPCG benchmark [5]. When it comes to distance-2 kernels popular methods seen in the literature are locking based methods, thread private local vectors [10, 6] for kernels like symmetric sparse matrix vector or with the usage of specially tailored sparse matrix data formats like compressed sparse blocks (CSB) [3] or recursive sparse blocks (RSB) [18].

3. Contribution. The paper focuses on developing an alternative method to parallelize kernels having loop-carried dependencies. The method introduced here is applicable for solving general distance- k dependencies, similar to multi-coloring methods. Currently we focus only on undirected graph i.e., matrices with symmetric sparsity pattern (but not necessarily symmetric entries). The main motivation of the approach is to achieve good hardware performance on modern hardware architecture, by generating sufficient parallelism while preserving good data locality. The method needs no specialized data format, and works basically on simple sparse matrix format like compressed row storage (CRS).

Most of the above approaches explained above in section 2 suffer from performance penalties in one way or the other, for example multi-coloring degrades the data locality, although this can be improved considerably using algebraic block multi-coloring, still for moderately large matrices or with the increase in k of distance- k dependency the method shows deterioration in performance. Similar drawbacks exists for other methods which will be discussed in detail within this paper.

In this work we provide a detailed performance analysis of the method and comparison between different existing methods chosen from representative classes. The comparisons are done both for exact kernels like symmetric sparse matrix vector (SymmSpMV) having distance-2 dependency and iterative solvers like Gauss-Seidel (GS) and Kaczmarz (KACZ) schemes having distance-1 and distance-2 dependencies respectively. For iterative schemes we further provide comparison between convergence of different methods. The comparisons are done on different hardware architectures ranging from Intel's Ivy-Bridge series to modern Sky-Lake architecture and the AMD Epyc architecture. The comparisons shows the superiority of our method compared to others and the applicability of our method on wide-variety of heterogeneous systems. As far to our knowledge this is the first paper which demonstrates such high efficiency of distance-2 dependent kernels using simple and common CRS matrix storage format on such broad scale of matrices.

The paper is limited to node level, and we use only thread level parallelization. Multi-node parallelization is left for future work. However it should be noted that for iterative kernels like KACZ and GS node-level performance is far more important because commonly such solvers are applied only locally and a different approaches are used for parallelizing between nodes [5, 11].

As a final application run we demonstrate the parallelization of an eigen-value solver called FEAST [21], where we use an iterative inner linear solver based on

Kaczmarz method. The result presented is the first to achieve such high performance on node level for an iterative solver and is superior to the previous results published [9].

4. Test bed, matrices and kernels.

4.1. Test bed. The tests are conducted on three different multi-core architectures. Two of them being Intel’s Ivy-Bridge and modern Sky-Lake architecture, the choice of these architectures enable study of the method on two extreme generation of Intel’s processor currently being used on HPC systems. As a third choice we select AMD’s recent Epyc architecture, which is competitive to Intel Sky-Lake architecture. This choice enables us to study the effect of our method on chips based on completely different microarchitecture, enabling us to demonstrate the applicability of our method on wide range of architectures. All the tests are conducted on a single socket of these architectures.

- Intel Ivy-Bridge architecture belongs to class of classic Intel’s cache-based architecture, which has three inclusive cache hierarchies. All the cache are scalable and the LLC (L3) being shared among all the cores on one socket. The processor is capable of delivering one full four wide SIMD add, multiply and load in one cycle.
- Intel Sky-Lake architecture belongs to recent generation of Intel family. Contrary to it’s predecessors (like Ivy-Bridge), the LLC is now changed to a non-inclusive victim cache shared by all the cores on a socket. The architecture comes with support for eight wide SIMD operations (AVX-512). The processor is capable of doing two AVX-512 add, multiply and load operations per cycle.
- AMD Epyc is based on AMD’s Zen microarchitecture. The basic building block of the architecture consists of Core Complex (CCX) consisting of three cores (can extend upto four on high end models) each having it’s own private L1 and L2 cache. The L3 cache is shared between a core complex and is non-inclusive victim cache. A single socket of Epyc consists of eight such core complexes.

The details of architectures along with the measured bandwidths are given in Table 1.

The bandwidths are measured using *likwid – bench* suite.

TABLE 1
Test bed

Model name	Xeon [®] E5-2660	Xeon [®] Gold 6148	Epyc 7451
Microarchitecture	Ivy Bridge	Skylake	Zen
Clock	2.2 GHz	2.4 GHz	2.3 GHz
Physical Cores per socket	10	20	24
L1d Cache	10 × 32 kB	20 × 32 kB	24 × 32 kB
L2 Cache	10 × 256 kB	20 × 1 MB	24 × 512 MB
L3 Cache	25 MB	27.5 MB	8 × 8 MB
L3 type	inclusive	non-inclusive	non-inclusive
Main Memory	32 GB	45 GB	4 × 16 GB
Bandwidth - load only	47 GB/s	115 GB/s	130 GB/s
Bandwidth - copy	40 GB/s	104 GB/s	114 GB/s
Architecture specific flag	-	-xCORE-AVX512	-

The code was compiled with newest Intel compiler version 17 and the following compiler flags were set `-fno-alias -xHost -O3`. Furthermore all the measurements

were done with CPU clock speeds fixed at frequencies indicated in Table 1.

4.2. External Tolls and Software.

- LIKWID
- ColPACK
- SpMP
- METIS

4.3. Benchmark Matrices. All the test matrices are taken from SuiteSparse Matrix Collection (former University of Florida Sparse Matrix Collection) [2] and quantum mechanics field (see ESSEX project [1] for more details). The selection of the matrices from SuiteSparse Matrix Collection is mainly done by combining the test matrices from two papers [18, 20]. This enables easy comparison of results. Matrices from ESSEX project are some of the matrices that are of interest in the FEAST eigen value solver. Only matrices having undirected graphs are considered due to scope of the paper as mentioned in section 3. Matrices along with some of their parameters are given in Table 2. Matrices that have been marked with an * symbol indicate they are corner cases and will be discussed in detail.

TABLE 2
Benchmark matrices

Index	Matrix name	nrows	nnz	nnzr	bandwidth		
1	audikw_1	943695	77651847	82.285	925946	*	SuiteSparse Matrix Collection
2	bone010	986703	71666325	72.632	13016		
3	channel-500x100x100-b050	4802000	85362744	17.776	600299		
4	crankseg_1	52804	10614210	201.011	50388		
5	delaunay_n24	16777216	100663202	6.0	16769102		
6	dielFilterV3real	1102824	89306020	80.979	1036475		
7	Emilia.923	923136	41005206	44.419	17279		
8	F1	343791	26837113	78.062	343754		
9	Fault_639	638802	28614564	44.794	19988		
10	Flan_1565	1564794	117406044	75.03	20702		
11	G3_circuit	1585478	7660826	4.832	947128		
12	Geo_1438	1437960	63156690	43.921	26018		
13	gsm_106857	589446	21758924	36.914	588744		
14	Hook_1498	1498023	60917445	40.665	29036		
15	HPCG-192	7077888	189119224	26.72	37057		
16	inline_1	503712	36816342	73.09	502403	*	SuiteSparse Matrix Collection
17	nlpkkt120	3542400	96845792	27.339	1814521		
18	nlpkkt200	16240000	448225632	27.6	8240201		
19	offshore	259789	4242673	16.331	237738		
20	parabolic_fem	525825	3674625	6.988	525820		
21	pwtk	217918	11634424	53.389	189331		
22	Serena	1391349	64531701	46.381	81578		
23	ship_003	121728	8086034	66.427	3659		
24	thermal2	1228045	8580313	6.987	1226000		
25	Anderson-16.5	2097152	14680064	7.0	1198372	*	ESSEX
26	Graphene-2048	4194304	16771072	3.999	2048		
27	Graphene-4096	16777216	67096576	3.999	4096		
28	Spin-26	10400600	145608400	14.0	709995		

4.4. Kernels. To test the performance we choose algorithms that are exact as well as iterative. Also we include kernels from both distance-1 and distance-2 dependency classes. All the kernels shown below are based on CRS matrix storage format.

147 **4.4.1. SpMV.** Sparse Matrix Vector (SpMV) is a kernel that do not have any
 148 dependencies. It acts as a good reference for other kernels to determine their perfor-
 149 mance upper bound.

Algorithm 4.1 SpMV Find $b : b = Ax$

```

1: for  $row = 1 : n_{rows}$  do
2:   for  $idx = rowPtr[row] : rowPtr[row + 1]$  do
3:      $b[row] += A[idx] * x[col[idx]]$ 
4:   end for
5: end for
```

150 The arithmetic intensity of the kernel I_{SpMV} is as follows:

151 (4.1)
$$I_{SpMV} = \frac{2}{8 + 4 + 8 * \alpha + \frac{16}{N_{n_{zr}}}}$$

152 where α represents the data locality factor and $N_{n_{zr}}$ non-zeros per row. α depends
 153 on the sparsity pattern of the matrix and varies from matrix to matrix. Ideal value
 154 of α for sufficiently large matrix is $\frac{1}{N_{n_{zr}}}$. More details on factor α could be found in
 155 [15].

156 **4.4.2. SpMTV.** Sparse Matrix Transpose Vector (SpMTV) is a kernel having
 157 distance-2 dependency.

Algorithm 4.2 SpMTV Find $b : b = A'x$

```

1: for  $row = 1 : n_{rows}$  do
2:   for  $idx = rowPtr[row] : rowPtr[row + 1]$  do
3:      $b[col[idx]] += A[idx] * x[row]$ 
4:   end for
5: end for
```

158 In comparison to SpMV operation, the kernel requires an extra scatter operation,
 159 which causes dependency. The arithmetic intensity of the kernel I_{SpMTV} is given as:

160 (4.2)
$$I_{SpMTV} = \frac{2}{8 + 4 + 16 * \alpha + \frac{8}{N_{n_{zr}}}}$$

161 In ideal case data traffic for this kernel should remain close to that of SpMV, if
 162 $N_{n_{zr}}$ are sufficiently high, and α factor is small enough.

163 **4.4.3. SymmSpMV.** Symmetric Sparse Matrix Vector (SymmSpMV) makes
 164 use of the symmetric property of the matrix to perform the matrix vector multiplica-
 165 tion.

Algorithm 4.3 SymmSpMV Find $b : b = Ax$, where A is an upper triangular matrix

```

1: for  $row = 1 : n_{rows}$  do
2:    $diag\_idx = rowPtr[row]$ 
3:    $b[row] += A[diag\_idx] * x[row]$ 
4:   for  $idx = rowPtr[row] + 1 : rowPtr[row + 1]$  do
5:      $b[row] += A[idx] * x[col[idx]]$ 
6:      $b[col[idx]] += A[idx] * x[row]$ 
7:   end for
8: end for

```

To operate on this kernel we just use the upper triangular part of the sparse matrix. The kernel requires only half the data traffic compared to SpMV but requires the same amount of Flops, leading to almost twice the intensity of SpMV operations.

$$(4.3) \quad I_{\text{SymmSpMV}} = \frac{4}{8 + 4 + 32 * \alpha + \frac{16}{N_{n,z,r}^{\text{symm}}}}$$

Note that $N_{n,z,r}^{\text{symm}}$ is the number of non-zeros per row in upper triangular part of the matrix.

4.4.4. GS and SymmGS. Gauss-Seidel (GS) is a solver having distance-1 dependency. Contrary to the above kernels GS is in-exact meaning it is an iterative method. Alg. 4.4 shows the Gauss-Seidel algorithm where its assumed that the diagonal entries of the matrix is stored as first entry in their corresponding rows.

Algorithm 4.4 GS Solve for $x : Ax = b$

```

1: for  $row = 1 : n_{rows}$  do
2:    $x[row] += b[row]$ 
3:   for  $idx = rowPtr[row] + 1 : rowPtr[row + 1]$  do
4:      $x[row] -= A[idx] * x[col[idx]]$ 
5:   end for
6:    $diag = A[rowPtr[row]]$ 
7:    $x[row] / = diag$ 
8: end for

```

Regarding the in-core execution the kernel has same properties as of SpMV, but requires an additional divide operation per row of the matrix. If the locality (α factor) is not disturbed due to pre-processing the kernel requires same data traffic as of SpMV. The arithmetic intensity of GS is the same as that of SpMV, if we neglect the divide operation that occurs once per every row.

$$(4.4) \quad I_{\text{GS}} = I_{\text{SPMV}}$$

In general for most of the algorithms one is interested in symmetric operator therefore commonly one would encounter symmetric variant of Gauss-Seidel, so called symmetric Gauss-Seidel (SymmGS). The algorithm remains same except that instead of just doing forward sweep shown in Algorithm 4.4 one would follow it with a backward sweep i.e., $row=n_{rows}-1:1$. The intensity of SymmGS remains same as of GS, as we do two times more flops and bring in proportional data.

188 **4.4.5. KACZ and SymmKACZ.** Kaczmarz (KACZ) is an iterative solver
 189 based on row-projection based methods. The solver has a distance-2 dependency.

Algorithm 4.5 KACZ Solve for $x : Ax = b$

```

1: for  $row = 1 : n_{rows}$  do
2:    $row\_norm = 0$ 
3:    $scale = b[row]$ 
4:   for  $idx = rowPtr[row] : rowPtr[row + 1]$  do
5:      $scale -= A[idx] * x[col[idx]]$ 
6:      $rownorm += A[idx] * A[idx]$ 
7:   end for
8:    $scale = scale / rownorm$ 
9:   for  $idx = rowPtr[row] : rowPtr[row + 1]$  do
10:     $x[col[idx]] += scale * A[idx]$ 
11:   end for
12: end for

```

190 In-core has a mixed behavior of both SpMV and SpMTV similar to SymmSpMV.
 191 The solver also requires a divide per row of the matrix. In ideal case the data traffic
 192 from memory should remain same as that of SpMTV. But the solver requires thrice
 193 the flops compared to SpMTV per non-zero. For brevity of the results we ignore the
 194 flops used in *rownorm* computations since, one could also row normalize the sparse
 195 matrix before performing the KACZ operation. This leads to an almost two fold
 196 higher Arithmetic Intensity compared to SpMTV.

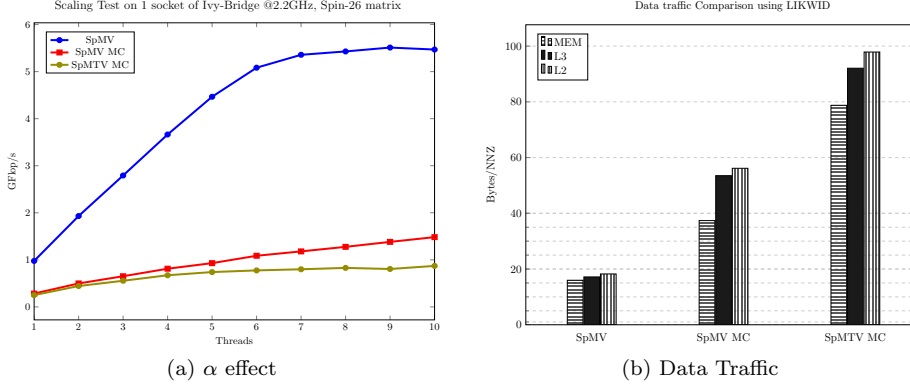
$$197 \quad (4.5) \quad I_{KACZ} = \frac{4}{8 + 4 + 16 * \alpha + \frac{8}{nnzr}} = 2 * I_{SpMTV}$$

198 Symmetric variant of KACZ is denoted by SymmKACZ, and similar to SymmGS
 199 this requires forward sweep followed by a backward sweep.

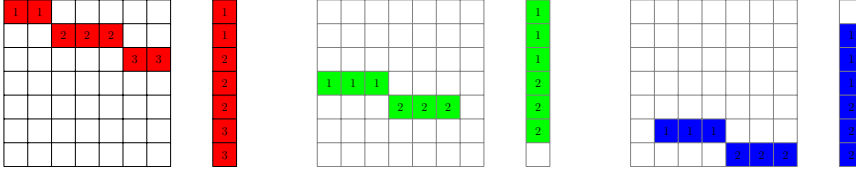
200 **5. Motivation.** Motivation for developing an alternative method stems from
 201 the ESSEX (Equipping Sparse Solvers for Exascale) project [1] where we investigate
 202 into solving large eigen-value problems from quantum mechanics field. In this context
 203 having a robust iterative solver was inevitable, due to the poor condition number
 204 of the matrices that appear in this field. Kaczmarz (KACZ) solver was found to
 205 be satisfactory but parallelizing this solver was deemed challenging because of the
 206 loop-carried dependencies in the kernel. Previous work on parallelizing the KACZ
 207 kernel used multi-coloring (MC) [9] but it was soon found that the kernels do not
 208 scale efficiently with this approach.

209 In order to get a better understanding of the underlying problem it's convenient
 210 to choose simple sparse matrix transpose vector (SpMTV) as a benchmark kernel.
 211 The particular choice of this kernel is due to the fact that both KACZ and SpMTV
 212 have similar kind of dependencies, and it's much easier to compare with our reference
 213 kernel namely sparse matrix vector (SpMV) which is embarrassingly parallel. The
 214 algorithm for SpMTV and SpMV has been listed in [Algorithms 4.1](#) and [4.2](#)

215 [Figure 1a](#) shows the performance of SpMV kernel on original unpermuted matrix
 216 and matrix with MC permutation. Here we see the performance of SpMV on multi-
 217 colored matrix is five times worse than that of SpMV on unpermuted matrix. One of
 218 the major reason for this drop is due to the increase in α factor seen in the intensity
 219 equation (4.2) Since the kernels like SpMV are mainly memory bound increase in

FIG. 1. *Effect of Multicoloring*

220 α lowers intensity I_{SpMV} leading to a drop of performance as predicted by roofline
 221 model [24]. This could easily be demonstrated by measuring the data traffic between
 222 different memory hierarchies. We do this using the LIKWID tool [23], and the mea-
 223 surements can be seen in Figure 1b. One can see an increase in data-traffic from all
 224 the memory hierarchy compared to SpMV on normal unpermuted matrix. This is
 225 basically caused by the bad data locality introduced by multi-coloring permutation.

FIG. 2. *Illustration of increase in α by multicoloring, numbers represents thread numbers working on a particular row*

226 Figure 2 shows an illustration of why data traffic increases for a given matrix. If
 227 one assumes last level cache (LLC) can only hold less than six elements and obeys
 228 perfect LRU policy, as seen in the Figure 2 for each new color we would need to load
 229 the data from main memory. As we will see later this α factor strongly depends on
 230 the matrix size and the size of LLC.

231 As seen in Figure 1b the data traffic further increases for SpMTV due to additional
 232 indirect writes (scatter) and this scales up α factor as seen in the denominator of
 233 I_{SpMTV} (see (4.2)), which further decreases performance of SpMTV compared to
 234 SpMV on MC matrix.

235 Other contributors to the drop in performance is global synchronizations and
 236 false sharing. These factors strongly depend on the number of colors and in general
 237 increase with chromatic number. For the Spin matrix the overhead of synchronization
 238 is roughly 10%. For most of the matrices one could also observe a strong positive
 239 correlation between false sharing and number of threads for SpMTV kernels, due to
 240 the indirect writes in SpMTV.

241 It was seen that for most of the matrices arising in the project average drop in
 242 performance by multi-coloring was almost a factor of two on a single socket of Ivy-
 243 Bridge. Although for most of them performance could be improved by algebraic block

multi-coloring (ABMC), still the results we obtained were not optimal (especially for large matrices) when compared to performance models which we will see later in section 8. This led to the development of a method which works on a common data format like CRS in which most of the other kernels are written and at the same time preserves data locality, reduce synchronization overheads and false sharing.

6. RACE method. Keeping in mind the observations from previous section 5, one could observe that it would be best to maintain the non-zeros of matrix close to the diagonal. This has been observed previously in the regard of normal sparse matrix computations like SpMV and has led to the pre-processing of matrix by applying bandwidth reduction algorithms like “Reverse Cuthill McKee ” (RCM). Now we aim to develop a method that does not distort this ideal permutations to a large extent but at the same time resolve distance- k dependencies.

Our approach can be seen as a recursive level based method. Each step of the method basically consists of four steps namely:

1. Level construction
2. Permutation
3. Distance- k coloring
4. Load balancing

The method is strongly coupled to the hardware underneath and exploits only the parallelism as required by the hardware. If at the end of all these four steps one does not achieve sufficient parallelism, all the steps are recursively applied to selected sub-graphs of the matrix until sufficient parallelism is attained. This recursive nature of our coloring method led to the naming of the method as “Recursive Algebraic Coloring Engine ” in short RACE .

To explain the method in an easier and illustrative way we choose a simple matrix namely the 2D 7pt. stencil. The sparsity pattern and the corresponding graph of the matrix is as shown in Figure 3.

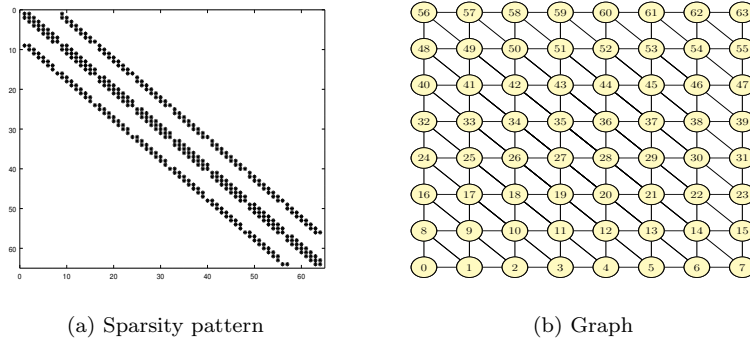


FIG. 3. 2d-7pt Stencil

Definitions. The following basic definitions from graph theory are used in the following sections:

- **Graph :** $G = (V, E)$ represents a graph where $V(G)$ belongs to set of vertices and $E(G)$ represents the edges in the graph. Note that here we specifically denote G for irreducible undirected graphs.
- **Neighborhood :** Neighborhood of vertex u represented as $N(u)$ is defined

as:

$$N(u) = \{v : uv \in E\}$$

- **Subgraph :** A subgraph H of graph G in this paper specifically refers to subgraph induced by $V' \subseteq V(G)$ and is defined as

$$H = (V', \{uv : uv \in E(G) \text{ and } u, v \in V'\})$$

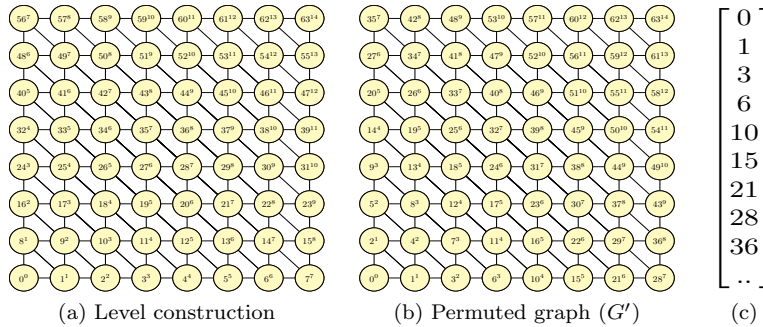
6.1. Level Construction. The first step of the RACE method is level construction. The step concerns with finding different *levels* in the graph, *levels* used here are same to the ones found in “Breadth First Search” (BFS) algorithm [16]. First *level* ($L(0)$) is chosen to consist of a selected root vertex. Rest of the levels ($L(i)$ for $i > 0$) are defined to contain vertices that are in neighborhood of vertices in previous *level* ($L(i-1)$) and not in $L(i-2)$ [4] i.e.,

$$L(i) = \begin{cases} u : u \in N(L(i-1)) \cap \overline{N(L(i-2))} & \text{if } i \neq 0 \\ \text{root} & \text{otherwise} \end{cases}$$

One could easily observe from (6.1) i -th *level* consist of all vertices that have a minimum distance of i from the root node. Algorithm A.1 shows an algorithm to find each nodes minimum distance from root. Total number of levels obtained with this graph traversal will be denoted as *total_level*. Figure 4a shows *levels* on the 2d-7pt stencil (*total_level* = 14), the main number on each vertex refers to the vertex number and the superscript shows the *level* number, i.e.,

$$n^i \implies n \in L(i)$$

Note that this is substantially different to the *levels* in methods like “level-scheduling” [22] where depth (maximum distance) is sought after.



node numbering between original lexicographic ordering in Figure 4a and Figure 4b. Now the most important step for resolving dependencies (coloring) is to store the information about *levels*. In order to do this we use a data structure called `level_ptr`. It stores the starting vector of each *levels*, which implies that *levels* on G' can be identified as:

$$L(i) = \{ u : u \in [\text{level_ptr}[i] : (\text{level_ptr}[i+1] - 1)] \text{ and } u \in V(G') \}$$

`level_ptr` for 2d-7pt stencil example is shown in Figure 4c, and one could easily read from `level_ptr` that vertices from `level_ptr(4) = 7` to `level_ptr(5) - 1 = 10` belongs to $L(4)$.

6.3. Distance- k coloring. Two vertices are called distance- k neighbours if the shortest path connecting them consists of at most k edges. This implies u is a distance- k neighbour of v (denoted as $u \xrightarrow{k} v$) if

$$(6.3) \quad u \xrightarrow{k} v \iff v \in \{ u \cup N(u) \cup N^2(u) \cup \dots \cup N^k(u) \}$$

Since we consider only undirected graph $u \xrightarrow{k} v$ also implies $v \xrightarrow{k} u$. After having the permuted graph G' one can show that $L(i)$ and $L(i+k+j)$ where $j \geq 1$ are distance- k independent as shown in the following Corollary 6.1:

COROLLARY 6.1. $L(i)$ and $L(i \pm (k+j))$ are distance- k independent $\forall j \geq 1$.

Proof. We prove by contradiction. Let there exist $u, v \in V(G')$ such that $u \in L(i)$ and $v \in L(i \pm (k+j)) \forall j \geq 1$. Assume u, v are distance- k neighbours ($u \xrightarrow{k} v$). From (6.1), (6.3) and the fact G' is undirected we get

$$\begin{aligned} u \xrightarrow{k} v &\iff v \in \{ L(i) \cup L(i \pm 1) \cup \dots \cup L(i \pm k) \} \\ &\implies v \notin L(i \pm (k+j)) \forall j \geq 1 \end{aligned}$$

which is a contradiction to the fact $v \in L(i \pm (k+j)) \forall j \geq 1$, this implies u and v are distance- k independent. \square

Corollary 6.1 implies that if we leave a gap of *at least* one *level* between any two *levels* ($L(i), L(i+2)$ for example) all the vertices between them are distance-1 independent. Similarly if there is a gap of *at least* two *levels* between any two *levels* ($L(i), L(i+3)$ for example) we get distance-2 independent levels.

Due to this weak definition in Corollary 6.1 there exists many possibility to make *levels* independent of each other and Figure 5 shows one such possibility each for distance-1 and distance-2 independent *levels*. One could group some of the nearby *levels* together to form a *level group*, and make this distance-1 or distance-2 independent of other *level groups*. The i -th *level group* would be denoted by $T(i)$. Difference between *level* and *level group* can be seen in Figure 5b, for Figure 5a *level group* and *level* coincides.

In principle one could compute on all independent *level groups* in parallel, but serial within a *level group*, i.e. for example in Figure 5b $T(0), T(2), T(4), T(6)$ can be operated by four different threads in parallel and in the next sweep rest *level groups*. For the configurations seen in Figure 5 this would mean we have $\frac{\text{total_level}}{2}$ and $\frac{\text{total_level}}{4}$ parallelism for distance-1 and distance-2 kernels respectively.

But the problem with the configurations like the one seen in Figure 5 is that there is load imbalances between threads as the number of rows (n_r) per *level group* is not

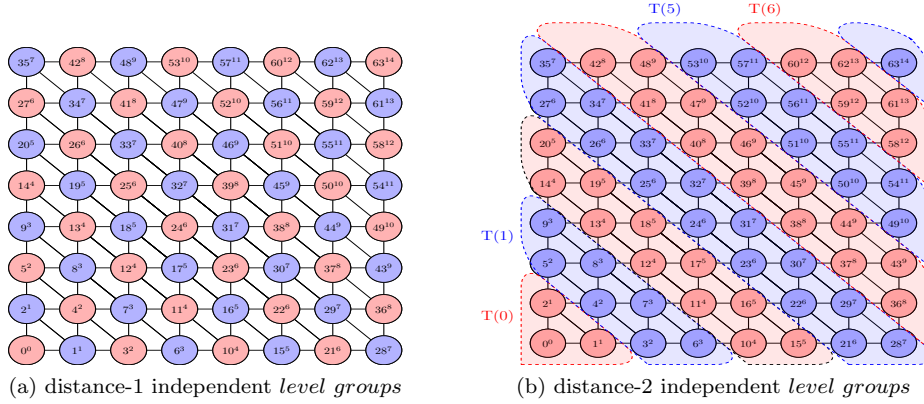


FIG. 5. distance-1 and distance-2 independent level groups.

distributed evenly. As seen here in the case of 2d-7pt stencil the threads working on extreme ends of graph (e.g., $T(1), T(7)$) have small amount of work compared to the threads working on middle (e.g., $T(3), T(4)$).

6.4. Load balancing. Depending on the matrix each *level group* would contain different number of rows, which leads to load imbalances as seen above in [subsection 6.3](#). In order to avoid this problem we employ a load balancing scheme. At this step we plug in detail from hardware side like total parallelism. The idea is to exploit only the parallelism as required by the hardware while at the same time maintain distance- k constraint seen in [Corollary 6.1](#). To balance the load more nearby *levels* would be added to a *level group* which has less number of n_r and at *level group* where we have considerably big *levels* only sufficient amount of *levels* to maintain distance- k constraint would be assigned. Assigning nearby levels instead of a random level further helps in preserving data locality.

An algorithm for load balancing can be found in [Algorithm A.2](#). The aim of the algorithm is to reduce combined variance of n_r in each *level group* ($T_size(i)$ refers to n_r in *level group* i). It does this by calculating mean and variance of T_size in each parallel sweeps. For example in [Figure 5b](#) we need to calculate mean of T_size of all *level groups* in red sweep and blue sweep separately. The combined variance is then found by summing up the variances in each parallel sweep. In order to reduce this combined variance we select the *level group* that has biggest absolute deviation from mean and try to add/remove levels to/from this *level group* from/to a *level group* that has biggest/least signed deviation. While removing *levels* from a *level group* one has to take care that the distance- k coloring is not violated, for example in case of distance-2 and two sweep scheme like seen in [Figure 5b](#) we need to ensure at least two levels remain in a *level group*. To aid this shifting of *levels* to/from *level group* we use the pointers to *level group* denoted by T_ptr . Doing this process in an iterative way finally we end up in a state with lowest combined variance at which no further moves are possible either due to violation of distance- k dependency or due to increase in combined variance. [Figure 6](#) shows step by step procedure involved in load balancing and [Figure 7](#) shows *level groups* after load balancing applied on 2d-7pt stencil example of size 16×16 .

One could also do this entire load balancing based on number of non-zeros (n_{nz}) rather than n_r .

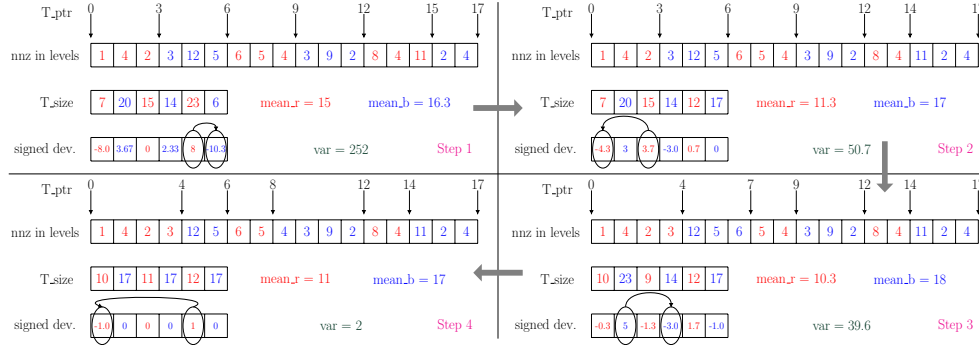
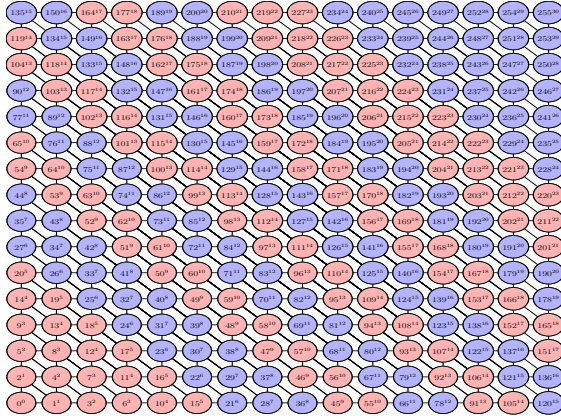


FIG. 6. Steps in load balancing (clockwise starting from top-left)

FIG. 7. After load balancing for five threads and distance-2 dependency on 2d-7pt stencil example, domain size 16×16 . Note that level groups at extreme end have more levels due to less n_r in each level, while level groups in middle having bigger levels maintain two levels to preserve distance-2 constraint.

6.5. Recursion. As seen above in subsection 6.3 maximum amount of parallelism by the above approach depends on *total_level*, also for most of the graphs as we approach the limit of parallelism there is not much room for load balancing, leading to imbalances. Depending on matrix and hardware underneath this might lead to inefficient utilization of resources. In order to avoid this problem we use the concept of recursion and exploit further parallelism if required by the hardware. Idea here is to intelligently select sub-graph(s) of the entire matrix and apply all the four steps recursively on this sub-graph. In the following we will show this concept in the context of distance-1 and later we will extent it to distance- k dependencies. Further we will discuss on the method employed to select proper sub-graph and to have a globally balanced load.

6.5.1. Distance-1. *Level groups* which we constructed till now belongs to stage 1 of recursion and to make the explanations easier the stage number of recursion would be denoted as subscript i.e., $L_s(i)$ denotes *level i* of stage s . Contrary to methods like multi-coloring we didn't require each nodes in a color to be distance-1 independent of each other rather we had a weak constraint as prescribed by Corollary 6.1. Due to this there can exist more parallelism within a *level group*. For example in Figure 8 we see that within third *level group* ($T_1(3)=L_1(3)$) vertices $4 \not\rightarrow 5$ (4 distance-1 independent to 5), $4 \not\rightarrow 6$, $4 \not\rightarrow 7$ and $5 \not\rightarrow 7$, implying each of these pairs can be

computed in parallel without any distance-1 conflicts. This parallelism couldn't be exploited in stage 1 since vertices in $L_1(k)$ (here $k=3$) were connected to preceding level $L_1(k-1)$ although some of them were not distance-1 dependent within $L_1(k)$. In order to exploit this parallelism we use the concept of recursion.

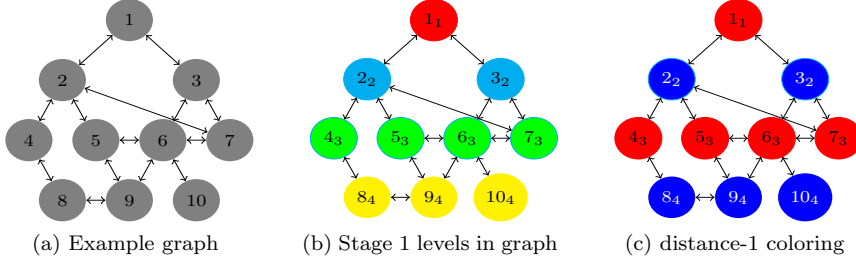


FIG. 8. Shows potential for more parallelism. $T_1(2), T_1(3)$ and $T_1(4)$ has more parallelism.

Recursion begins by selection of a sub-graph of the matrix. A typical choice is a sub-graph induced by vertices in a *level group* of previous stage, more on the selection of sub-graph will be seen later in subsection 6.5.4. For example let's choose sub-graph induced by $T_1(3)$ for recursion. The chosen sub-graph can be isolated from rest of the graph since distance-1 coloring step in stage 1 has already made *level groups* in a sweep independent of each other. Now we just need to repeat all the four step explained previously (subsection 6.1 - subsection 6.4) to exploit parallelism within this sub-graph.

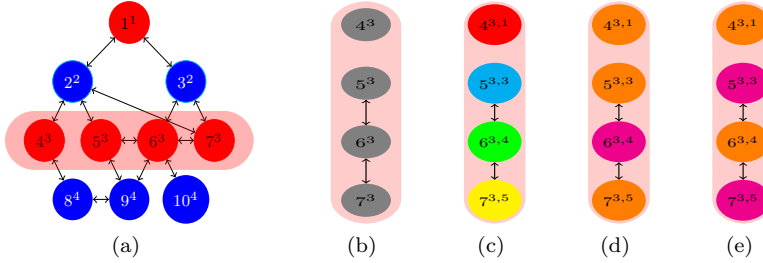


FIG. 9. Shows recursion being applied to $T_1(3)$. Figure 9b shows the selected sub-graph, Figure 9c shows level construction step on the sub-graph, Figures 9d and 9e shows two possibility of distance-1 coloring of the sub-graph

Figure 9 shows an illustration of applying stage 2 of recursion on $T_1(3)$ to find more parallelism. To incorporate the information of levels after recursion we extent the definition in (6.2) to the following:

$$(6.4) \quad n^{i,j,k,\dots} \implies n \in \{L_1(i) \cap L_2(j) \cap L_3(k) \cap \dots\}$$

Note that the sub-graphs might have multiple islands (group of vertices in a graph that are not connected to rest of the graph). For example vertex 4 in Figure 9b is an island in the considered sub-graph, similarly vertices 5,6,7 combine to form an island. Since an island is totally disconnected from the rest of the graph it can be executed in parallel to rest of the graph. To take advantage of this the starting node in next island is assigned with an increment of two levels, as seen in Figure 9c. Due to

this there exists multiple valid distance-1 configuration (here Figures 9d and 9e) and the selection of the optimum one will be done in the final load balancing step of a particular stage as described in subsection 6.4.

With this recursive process we were able to find independent *level groups* (T_{s+1}) within *level group* of previous stage (T_s) and therefore the thread which works on T_s has to spawn threads to parallelize within T_{s+1} .

6.5.2. Distance- k . For distance- k the same procedure as distance-1 applies, except with a slight difference in selecting the sub-graph. In distance-1 we considered sub-graphs induced by *level groups*, but for distance- k coloring this is not sufficient. As seen in Figure 10 for distance-2 coloring the selection of $T_1(2)$ as sub-graph did not guarantee distance-2 independency between *level group* T_2 within the sub-graph. This is due to the fact for $k > 1$ dependency vertices a, b within a sub-graph might be connected to a common vertex (c) outside the sub-graph leading to a distance- k dependency between a and b . In Figure 10 we see $4 \xrightarrow{1} 2$ & $7 \xrightarrow{1} 2 \implies 4 \xrightarrow{2} 7$, but since vertex 2 was not in the sub-graph considered we missed this dependency.

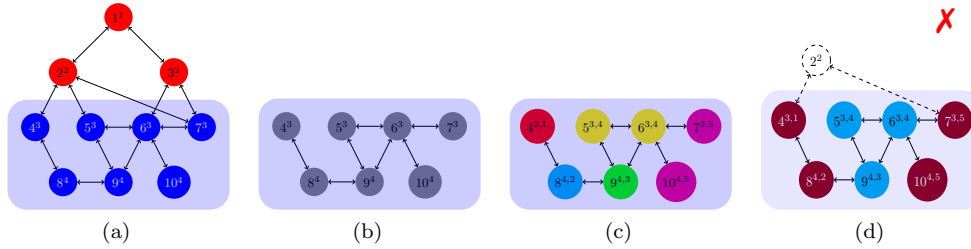


FIG. 10. Figures 10a and 10b shows *level group* induced sub-graph selected for recursion in case of distance-2. But applying the four steps to this selected sub-graph does not guarantee a distance-2 independency between *level group* of same sweep (color) as seen in Figure 10d

In order to resolve such dependency we have to consider an extra $(k-1)^{th}$ interface level(s) of the selected sub-graph for the level construction step. k^{th} interface level of subgraph $L_s(j)$, denoted as $I^k(L_s(j))$, is defined as follows:

$$I^k(L_s(j)) = \{ u : u \xrightarrow{k} v \forall v \in L_s(j) \text{ and } u \notin L_s(j) \}$$

For distance-2 this would mean we have to include 1 interface level, the new selection is illustrated in Figure 11. With the new sub-graph selection for distance-2 coloring as seen in Figure 11a, the result after third step distance- k coloring remains correct. In the example vertices 4 and 7 which had same color previously now gets a different color in (see Figure 11d).

Note that the interface levels have to be considered only in the first step namely level construction in the rest of the steps we just need to consider target sub-graphs induced by *level groups*.

6.5.3. level_tree. By recursion we are able to exploit more parallelism. However this introduces more complexity and one has to also respect the dependencies between stages in addition to one within stages. The best idea is to have a data structure similar to the recursion, therefore we extent the `level_ptr` data structure to a hierarchical tree data structure to store the informations. This data structure is called a `level_tree`. The root of `level_tree` contains information of entire domain,

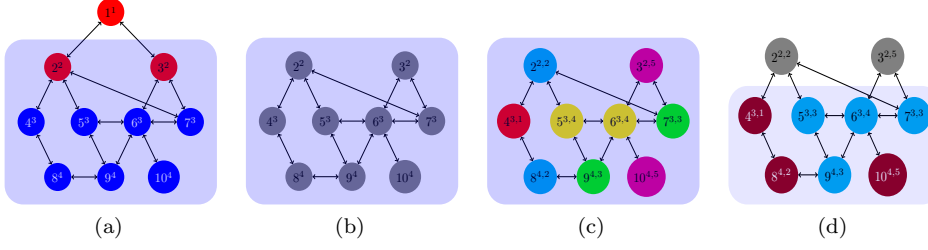


FIG. 11. Correct procedure of selecting sub-graph for distance-2 coloring. The level group $T(2)$ and its 1st interface level is chosen as shown in Figures 11a and 11b for level construction stage seen in Figure 11c. For rest of the steps only required sub-graph to be parallelised is considered as shown in Figure 11d for distance-k coloring.

first leaves of this root stores information about *level groups* in stage 1 (T_1), next
leaves about *level groups* in stage 2 (T_2) and so on.

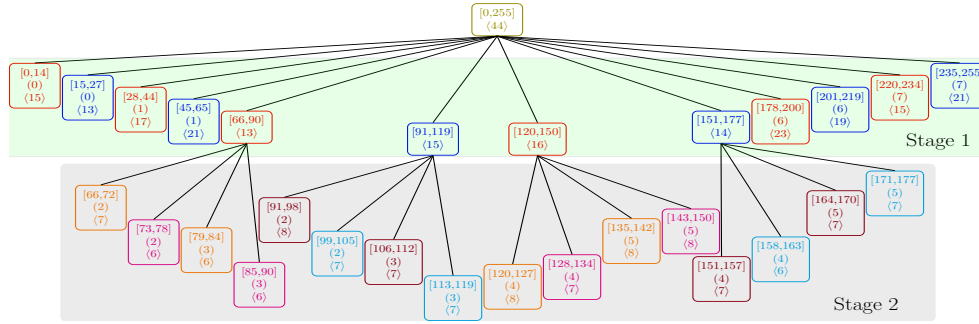
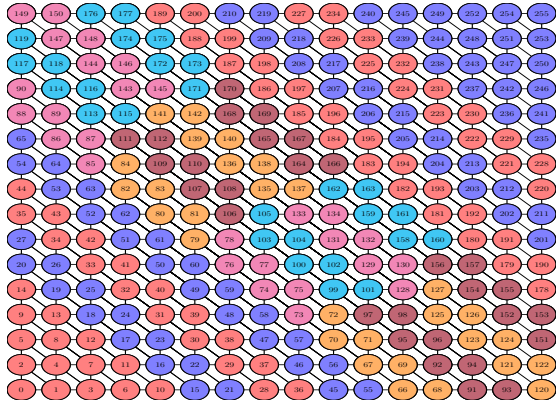


FIG. 12. `leveltree` corresponding to 2d-7pt stencil example for domain size 16×16 , and 8 threads. The range (square brackets) specified in each leaves represent the vertices belonging to each level group, the number in bracket (parenthesis) represents the thread assigned to the level group in fill type pinning and the n_r^{eff} (see section 7) is represented within angle brackets.



for parallel all red
for parallel all orange
for parallel all pink
for parallel all blue
for parallel all brown
for parallel all cyan

FIG. 13. Graph corresponding to `leveltree` in Figure 12. The execution order of different level group is specified in the short code snippet on right. Note nested parallelism being used.

Figure 12 shows a `leveltree` corresponding for 2d-7pt stencil example. Threads
are assigned to each *level group*, order of which depends on the pinning strategy
used. For example in fill type pinning strategy one would pin thread 0 to $T_1(0)$

and $T_1(1)$, thread 1 to $T_1(2)$ and $T_1(3)$, thread 2 to $T_2(0) \subset T_1(4)$, $T_2(1) \subset T_1(4)$, $T_2(0) \subset T_1(5)$ and $T_2(1) \subset T_1(5)$, and so on. In order to replicate this tree like parallelisation strategy we use nested parallelism, where threads in stage $k + 1$ is spawned by threads in stage k . The graph corresponding to 2d-7pt stencil example is shown in Figure 13, and the execution order is specified in the figure. At the end of each `for parallel all color` there is synchronization between threads assigned to *level group* of corresponding color. Since each of the leaf need to synchronize only with it's siblings (leaves of same parent) we use simple point to point synchronization scheme.

6.5.4. Sub-graph selection and global load balancing. Parallelism required for hardware underneath can be obtained either by expanding the `level_tree` horizontally i.e., increasing *level groups* within a stage or by expanding `level_tree` vertically with the help of recursion. But as we have seen before in subsection 6.3 the horizontal parallelism is limited and after a certain extent this would lead to load balancing. Similarly excessive usage of recursion is also not a good idea since data locality worsens due to local permutations within sub-graph. Therefore it is vital to find a proper balance and choose proper configuration. Furthermore just doing load balancing within a single stage is not the best, for example if we had equally balanced within stage 1 in Figure 12, we would receive no benefit from recursion. Therefore a global load balancing becomes inevitable.

In order to select proper sub-graph and do global load balancing we employ a simple algorithm to find proper weights for each *level group* ($T_s(i)$) in a particular stage, then depending on this weights, denoted as $w(T_s(i))$, we do load balancing with weights in the particular stage (as seen in Algorithm A.2, except weightage is given to *level groups*). Finally if $w(T_s(i)) > 1$ we use recursion to achieve $w(T_s(i))$ parallel work in the next stage of $T_s(i)$. The basic structure of the algorithm employed to find weights is as follows:

1. Find weights, $w(L_s(i))$ for each level in the current stage (s) by

$$w(L_s(i)) = (\text{level_ptr}_s[i + 1] - \text{level_ptr}_s[i]) * \frac{n_t}{n_r}$$

n_t : total parallelism required by hardware

n_r : number of vertices in graph

2. Starting from $w(L_s(0))$ sum up weights till they form a number (a) close to whole number (b). The closeness can be controlled by an efficiency parameter for stage s , ϵ_s is defined as:

$$(6.5) \quad \epsilon_s = 1 - \text{abs}(a - b);$$

The obtained number b is chosen as weight for *level groups* operated by first thread in the current stage i.e., $w(T_s(0)) = w(T_s(1)) = b$. A local search is then done by increasing *levels* in this *level groups* to see if there is a better choice (a close to b) with weight b , finally a *level group* is formed with the best choice. The weight for next *level groups* are found by resetting the sum counter to zero and repeating the procedure with *levels* just after the current *level groups*.

7. Parameter study. In this section we study the impact of parameter ϵ_s and hardware parallelism on the quality of RACE method. In order to do this we first quantify the quality of the method and finally we use this quantity to do a parameter

study. The study gives insights into tuning of parameter ϵ_s based on the given matrix and required parallelism.

7.1. Quantifying quality of RACE. Quantifying quality of the method in a well-defined way is a primary and most vital step for parameter study. We do this using the concept of *effective parallelism*. From [section 6](#) we saw that even though one tries to achieve parallelism exactly as that required by the hardware, in practice one might not be able to utilize this parallelism to 100 % due to load imbalances. Therefore we use a simple calculation based on the `level_tree` to determine efficiency, taking into account load imbalances from different stages of recursion. So we first calculate *effective row* for each of the finest leaves (worker leaves) in `level_tree`. *Effective row* for each worker leaf is the same as number of rows (n_r) on which each leaf has to operate, for example in case of $T_1(0)$ *effective row* ($n_r^{eff}(T_1(0))$) is 14 and $n_r^{eff}(T_2(0) \subset T_1(4))$ is 6. After calculating the *effective row* for worker leaves the information is propagated to lower stages (up in the `level_tree`) as follows:

$$n_r^{eff}(T_s(i)) = \max(n_r^{eff}(T_{s+1}(j) \subset T_s(i))) + \max(n_r^{eff}(T_{s+1}(k) \subset T_s(i)))$$

for j is even and k is odd

Such a definition for *effective row* is based on the idea that a parent has to wait until the child leaf with most number of rows has finished its work due to synchronization needed with its siblings. This has to be handled separately for each of the two parallel sweep as there is this synchronization happening after each of the sweeps.

Once the information is propagated up the tree and as it reaches the root we have a single *effective row* ($n_r^{eff}(T_0)$) for the entire tree, which has taken care of load balancing happening between all *level groups* in all stages. The ratio of total number of rows in the entire matrix to that of $n_r^{eff}(T_0)$ gives *effective parallelism*, denoted as n_t^{eff} . Efficiency (η) of the method is then defined as ratio of n_t^{eff} to that of required hardware parallelism (n_t).

$$(7.1) \quad n_t^{eff} = \frac{n_r}{n_r^{eff}(T_0)}$$

$$(7.2) \quad \eta = \frac{n_t^{eff}}{n_t}$$

For example in our 2d-7pt stencil example, [Figure 12](#) shows n_r^{eff} for each leaves in angular brackets and here $n_t^{eff} = 5.8$ and $\eta = 0.725$. The value of $\eta = 1$ implies there is perfect load balancing, else $0 < \eta \leq 1$. This parameter η will be used as a measure of quality in parameter study.

7.2. Case study. A given matrix has a fixed amount of parallelism and as the amount of required parallelism (n_t) increases load balancing degrades due to more threads per stage and imbalances between stages. The rate of degradation can however be controlled to certain extent by the tolerance ϵ_s (see [\(6.5\)](#)) specified while choosing a *level group*. Typical value of ϵ_s is in range of $[0.4, 0.9]$. Having a small ϵ_s (for example 0.4) implies we utilize the current stage ‘s’ to maximum and do not impose high load balancing constraint, a high value on the other hand requires more balanced load from current stage ‘s’.

Test matrices (see [section 4](#)) considered have a varying degree of parallelism, and in order to see the effect of η and ϵ_s we choose *inline* matrix. The choice is due to the

fact that this matrix has relatively small amount of parallelism and this allows us to demonstrate various effect, ranging from good to bad case scenario with small number of parallelism ($n_t < 200$). This limited parallelism can be observed from Figure 14a where efficiency keeps on decreasing with n_t for *inline* matrix. Similar behavior can be observed for *crankseg-1*, *F1* and *ship* matrices, of which *crankseg-1* being the worst. For majority of other test matrices one could observe that efficiency η initially drops but then remains almost constant in the range $\eta = [0.50, 0.80]$ (depending on matrix) for the entire scanned area of $1 \leq n_t \leq 200$.

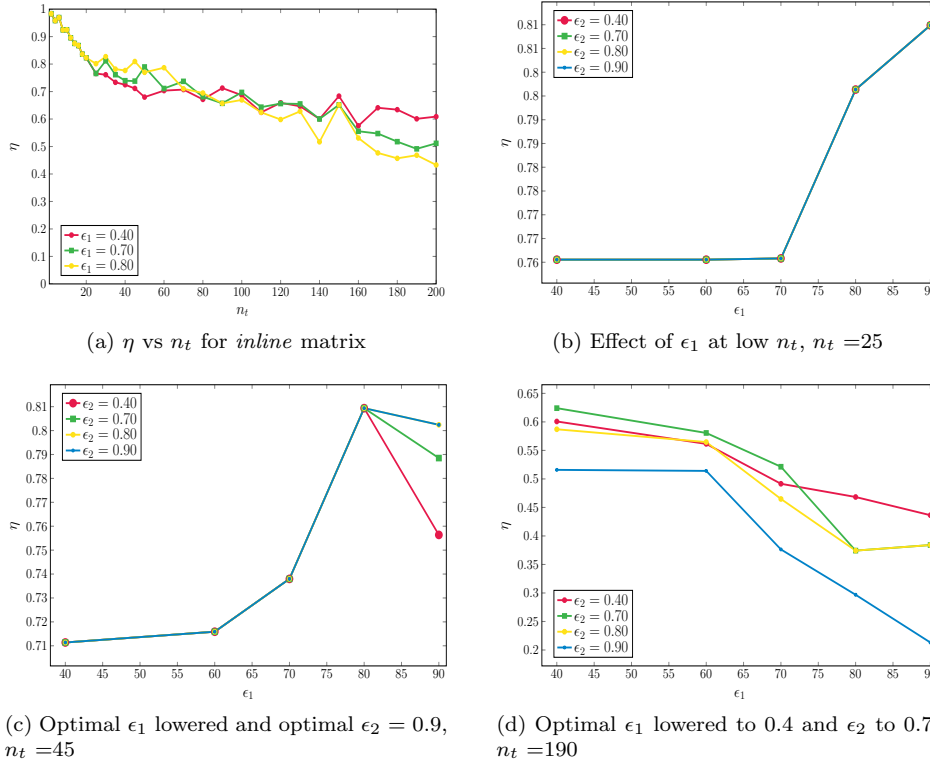


FIG. 14. Parameter study on *inline* matrix. In Figures 14b to 14d each lines in the plot are *iso- ϵ_2* and impact of η with respect to ϵ_1 is shown.

At small number of threads (n_t) all matrices have high efficiency (like $\eta > 0.8$). As there is a lot of parallelism in this stage compared to requirement, η is insensitive of ϵ_s . The value of n_t upto which such a behavior can be observed varies from matrix to matrix, for example *inline* shows this upto $n_t \approx 20$, while for matrix like *Graphene* this is grater than 200. Further increasing n_t one could then observe η starts to vary with ϵ_1 . For example in case of $n_t = 25$ one could see in Figure 14b maximum η is achieved with high value of ϵ_1 (0.9) due to good load balancing. But as n_t further increase the optimal ϵ_1 starts shifting towards left (see Figure 14c), since one requires more parallelism from the current stage ($s=1$) and higher ϵ_1 would be decremental since it would require the *level_tree* to go more deep and hence load imbalances in next stages will get multiplied. ϵ_2 which till now didn't effect much starts to influence slowly as n_t increments again, for example in case of *inline* till *nthreads* = 90 $\epsilon_2 = 0.9$ was optimal, but then the optimal ϵ_2 reduces and reaches 0.7 at $n_t = 190$

as seen in Figure 14d. η would start to get affected by ϵ_s of next stages in similar manner with increase of n_t .

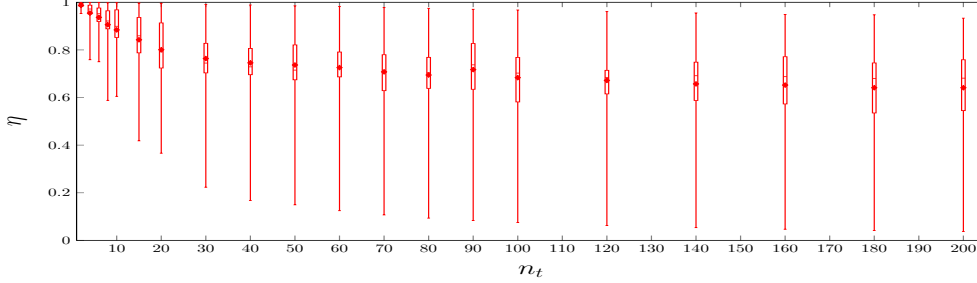


FIG. 15. Statistical box plot of η vs n_t of all test matrices, with $\epsilon_s = 0.4$

Behavior of other matrices in the test bed follow similar pattern, but n_t at which different phases occur varies from matrix to matrix. Figure 15 gives a broad overview of behavior of entire test matrices using statistical box plot. Majority of test matrices having an initial drop in η and then remaining constant is reflected in the statistical plot. The lowest whisker in the plot corresponds to *crankseg_1* matrix, here we achieve only a mere parallelism of eight at maximum ($n_t^{eff} = 8$), while the upper whisker corresponds to matrix having highest parallelism namely *Graphene* matrix.

In practice for a given matrix it's difficult to precisely determine the optimal rate of decrease in ϵ_s without parameter search, and therefore selecting proper ϵ_s for given n_t can be challenging. One idea is to see the *total_level* and distribution of n_r (or n_{nz}) in different levels of current stage 's' and heuristically determine ϵ_s based on the pressure of parallelism from stage 's'. This is not currently done and is part of our future work. Currently for experiments we set $\epsilon_s = 0.8$ for all matrices.

In Figure 16 we have plotted n_t^{eff} and η vs n_t for corner case matrices with the settings used in experiment runs. Here we set $\epsilon_{1,2} = 0.8$ and use RCM (Reverse Cuthill McKee) in the *level construction* stage (subsection 6.1). Big fluctuation in *crankseg_1* is due to the fact that we set high load balancing requirement (high ϵ_s factor) and as seen in the example of *inline_1* matrix this is not optimal when we reach the limit of parallelism. The theoretical estimated obtained in Figure 16 will be directly used to compare with experiment runs in the next section (section 8).

8. Experiments and Results. The method stated above was implemented and consolidated into a library called RACE. The library provides easy interface for parallelizing kernels, user typically just needs to supply the serial code (with dependency) and hardware settings. Library will then parallelize, pin and run the code in parallel. The library is publicly available in the git repository.

8.1. Test setup. In the following we present the performance and convergence results obtained using the library, and compare it against state of art methods. Hardware and matrices as described in section 4 is used for the following benchmarks. As mentioned in section 7 parameter ϵ_s is set to 0.8 and RCM is used in level construction stage. All the experiments conducted here are using warmed up caches i.e., we run the kernel for 100 times initially for warm-up and then we measure performance for the next 500 iteration of the same kernel. Mean performance of this 500 iterations is used to plot the results.

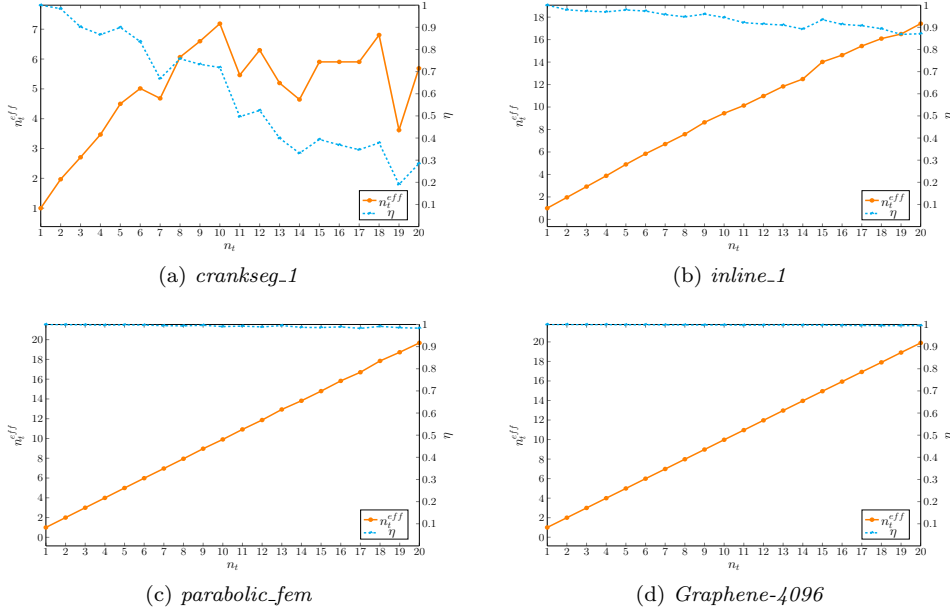


FIG. 16. n_t^{eff} and η vs n_t for corner case matrices, with the same settings used in experiment runs.

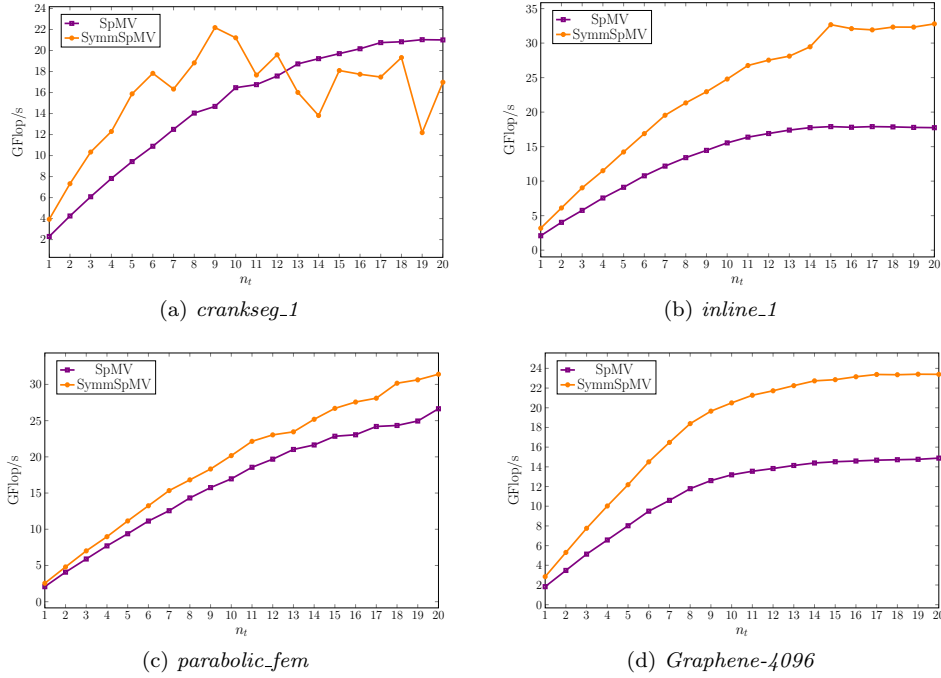


FIG. 17. Scaling of SymmSpMV with RACE compared to SpMV on one socket of Sky-Lake architecture, for corner case matrices.

8.2. Corner Cases. Figure 17 shows the scaling performance of SymmSpMV for the corner case matrices on one socket of Sky-Lake architecture. The *crankseg_1* matrix does not scale well due to its limited parallelism, as seen in Figure 16a, one could further see that the scaling behavior Figure 17a is exactly in tune with that of the theoretical result seen in Figure 16a. Note that due to this bottleneck of parallelism we didn't achieve much benefit from using SymmSpMV compared to SpMV.

The *inline_1* matrix although being third lowest in terms of parallelism in the entire set of test matrices, but it still achieves a high efficiency ($\eta = 0.85$) for 20 threads (see Figure 16b), leading to good scaling as seen in Figure 17b. The saturation in performance after 15 threads is due to the fact that we hit the memory bottleneck, similar behavior can also be observed for SpMV which is embarrassingly parallel. The saturation occurs at the maximum achievable performance on the given architecture which could easily be verified using the roofline model ([24]) as shown below:

$$\begin{aligned}
 P_{max} &= 2 \left[\frac{\text{FMA AVX-512 instruction}}{\text{cy} * \text{cores}} \right] * 8 \left[\frac{\text{FMA}}{\text{FMA AVX-512 instruction}} \right] \\
 &\quad * 2 \left[\frac{\text{Flop}}{\text{FMA}} \right] * 2.4 \left[\frac{\text{Gcy}}{\text{s}} \right] * 20 [\text{cores}] = 1536 \left[\frac{\text{GFlop}}{\text{s}} \right] \\
 I_{\text{SpMV}} &= \frac{2}{8 + 4 + \frac{8+16}{73}} = 0.162 \left[\frac{\text{Flop}}{\text{byte}} \right], \text{ assuming best case : } \alpha = \frac{1}{N_{n\text{zr}}} \\
 P_{\text{SpMV}} &= \min(P_{max}, b_s * I_{\text{SpMV}}) \\
 P_{\text{SpMV}} &= \min(1536, 0.162 * 115) = 18.6 \left[\frac{\text{GFlop}}{\text{s}} \right]
 \end{aligned}$$

As seen we achieve 17.8 GFlop/s which is close to the theoretical maximum of 18.6 GFlop/s for SpMV. Similar derivation can be done for SymmSpMV and one could see $P_{\text{SymmSpMV}} = 34.5$ GFlop/s, which is approximately twice that of SpMV since I_{SymmSpMV} is almost a factor two higher than I_{SpMV} for matrix with moderate $N_{n\text{zr}}$. From Figure 17b one can observe that at saturation we reach close to theoretical values. The cushioning effect of memory bandwidth bottleneck is also evident from Figure 17b, where we see that due to this saturation decrease in η to a certain extent would not effect the socket level performance, it would just shift the knee of saturation towards right.

In the case of *parabolic_fem* matrix we theoretically have a good efficiency as seen from Figure 16c, but here we do not see any saturation in performance (see Figure 17c), even SpMV does not have this saturation behavior. If one calculates the maximum theoretical performance by roofline model as shown in previous example one would see that $P_{\text{SpMV}} = 15$ GFlop/s and $P_{\text{SymmSpMV}} = 19$ GFlop/s, but we achieve more than these values 26.5 and 31.5 GFlop/s respectively, this is because the matrix is small enough (≈ 46 MB for full matrix and ≈ 23 MB for symmetric storage) and it just fits in caches (combined L2 and L3) of the Sky-Lake architecture. Since the caches scales well on this architecture we don't observe the saturation behavior. Also observe that difference between SymmSpMV and SpMV is not two times here since non-zeros per row is small ($N_{n\text{zr}} = 7$, $N_{n\text{zr}}^{\text{symm}} = 4$).

Graphene-4096 matrix on the other hand is a matrix with efficiency similar to *parabolic_fem* but with much larger size ($\approx 2GB$) resulting in matrix data always coming from main memory. This therefore shows dominant saturation behavior and since we achieve good efficiency (η) the knee of saturation begins at a well early stage for SymmSpMV compared to the case of *inline_1* where the efficiency was lower in comparison resulting in smaller n_t^{eff} .

651 **9. Application Runs.**

652 **10. Conclusion.**

653 **11. Future Work.**

654 **Acknowledgments.** We would like to acknowledge the assistance of volunteers
655 in putting together this example manuscript and supplement.

REFERENCES

- [1] *Equipping Sparse Solvers for Exascale - ESSEX*. <https://blogs.fau.de/essex/activities>.
- [2] *SuiteSparse Matrix Collection*. <https://sparse.tamu.edu/>.
- [3] A. BULUÇ, J. T. FINEMAN, M. FRIGO, J. R. GILBERT, AND C. E. LEISERSON, *Parallel sparse matrix-vector and matrix-transpose-vector multiplication using compressed sparse blocks*, in Proceedings of the Twenty-first Annual Symposium on Parallelism in Algorithms and Architectures, SPAA '09, New York, NY, USA, 2009, ACM, pp. 233–244, <https://doi.org/10.1145/1583991.1584053>.
- [4] J. DÍAZ, J. PETIT, AND M. SERNA, *A survey of graph layout problems*, ACM Comput. Surv., 34 (2002), pp. 313–356, <https://doi.org/10.1145/568522.568523>.
- [5] J. DONGARRA AND M. HEROUX, *Toward a new metric for ranking high performance computing systems*, Tech. Report SAND2013-4744, Sandia National Laboratories, 2013.
- [6] A. ELAFROU, V. KARAKASIS, T. GKOUNTOUVAS, K. KOURTIS, G. GOUMAS, AND N. KOZIRIS, *Sparsex: A library for high-performance sparse matrix-vector multiplication on multicore platforms*, ACM Trans. Math. Softw., 44 (2018), pp. 26:1–26:32, <https://doi.org/10.1145/3134442>.
- [7] T. ELFVING, *Block-iterative methods for consistent and inconsistent linear equations*, Numerische Mathematik, 35 (1980), pp. 1–12, <https://doi.org/10.1007/BF01396365>, <https://doi.org/10.1007/BF01396365>.
- [8] D. J. EVANS, *Parallel S.O.R. Iterative Methods*, Parallel Comput., 1 (1984), pp. 3–18, [https://doi.org/10.1016/S0167-8191\(84\)90380-6](https://doi.org/10.1016/S0167-8191(84)90380-6).
- [9] M. GALGON, L. KRÄMER, J. THIES, A. BASERMANN, AND B. LANG, *On the parallel iterative solution of linear systems arising in the fast algorithm for computing inner eigenvalues*, Parallel Comput., 49 (2015), pp. 153–163, <https://doi.org/10.1016/j.parco.2015.06.005>.
- [10] T. GKOUNTOUVAS, V. KARAKASIS, K. KOURTIS, G. GOUMAS, AND N. KOZIRIS, *Improving the performance of the symmetric sparse matrix-vector multiplication in multicore*, in 2013 IEEE 27th International Symposium on Parallel and Distributed Processing, May 2013, pp. 273–283, <https://doi.org/10.1109/IPDPS.2013.43>.
- [11] D. GORDON AND R. GORDON, *Component-averaged row projections: A robust, block-parallel scheme for sparse linear systems*, SIAM Journal on Scientific Computing, 27 (2005), pp. 1092–1117, <https://doi.org/10.1137/040609458>.
- [12] T. IWASHITA, H. NAKASHIMA, AND Y. TAKAHASHI, *Algebraic block multi-color ordering method for parallel multi-threaded sparse triangular solver in iccg method*, in Proceedings of the 2012 IEEE 26th International Parallel and Distributed Processing Symposium, IPDPS '12, Washington, DC, USA, 2012, IEEE Computer Society, pp. 474–483, <https://doi.org/10.1109/IPDPS.2012.51>, <http://dx.doi.org/10.1109/IPDPS.2012.51>.
- [13] M. T. JONES AND P. E. PLASSMANN, *Scalable iterative solution of sparse linear systems*, Parallel Comput., 20 (1994), pp. 753–773, [https://doi.org/10.1016/0167-8191\(94\)90004-3](https://doi.org/10.1016/0167-8191(94)90004-3), [http://dx.doi.org/10.1016/0167-8191\(94\)90004-3](http://dx.doi.org/10.1016/0167-8191(94)90004-3).
- [14] C. KAMATH AND A. SAMEH, *A projection method for solving nonsymmetric linear systems on multiprocessors*, 9 (1989), pp. 291–312, [https://doi.org/10.1016/0167-8191\(89\)90114-2](https://doi.org/10.1016/0167-8191(89)90114-2).
- [15] M. KREUTZER, G. HAGER, G. WELLEIN, H. FEHSKE, AND A. R. BISHOP, *A Unified Sparse Matrix Data Format for Efficient General Sparse Matrix-Vector Multiplication on Modern Processors with Wide SIMD Units*, SIAM Journal on Scientific Computing, 36 (2014), pp. C401–C423, <https://doi.org/10.1137/130930352>.
- [16] C. Y. LEE, *An algorithm for path connections and its applications*, IRE Transactions on Electronic Computers, EC-10 (1961), pp. 346–365, <https://doi.org/10.1109/TEC.1961.5219222>.
- [17] H. LU, M. HALAPPANAVAR, D. CHAVARRA-MIRANDA, A. H. GEBREMEDHIN, A. PANYALA, AND A. KALYANARAMAN, *Algorithms for balanced graph colorings with applications in parallel computing*, IEEE Transactions on Parallel and Distributed Systems, 28 (2017), pp. 1240–1256, <https://doi.org/10.1109/TPDS.2016.2620142>.
- [18] M. MARTONE, *Efficient multithreaded untransposed, transposed or symmetric sparse matrix-vector multiplication with the recursive sparse blocks format*, Parallel Comput., 40 (2014), pp. 251–270, <https://doi.org/10.1016/j.parco.2014.03.008>, <http://dx.doi.org/10.1016/j.parco.2014.03.008>.
- [19] K. NAKAJIMA AND H. OKUDA, *Parallel iterative solvers for unstructured grids using an openmp/mpi hybrid programming model for the geofem platform on smp cluster architectures*, in High Performance Computing, H. P. Zima, K. Joe, M. Sato, Y. Seo, and M. Shimasaki, eds., Berlin, Heidelberg, 2002, Springer Berlin Heidelberg, pp. 437–448.
- [20] J. PARK, M. SMELYANSKIY, N. SUNDARAM, AND P. DUBEY, *Sparsifying synchronization for high-performance shared-memory sparse triangular solver*, in Proceedings of the 29th

- International Conference on Supercomputing - Volume 8488, ISC 2014, New York, NY, USA, 2014, Springer-Verlag New York, Inc., pp. 124–140, https://doi.org/10.1007/978-3-319-07518-1_8.
- [21] E. POLIZZI, *A density matrix-based algorithm for solving eigenvalue problems*, CoRR, abs/0901.2665 (2009), <https://arxiv.org/abs/0901.2665>.
- [22] Y. SAAD, *Iterative Methods for Sparse Linear Systems*, Society for Industrial and Applied Mathematics, second ed., 2003, <https://doi.org/10.1137/1.9780898718003>, <https://epubs.siam.org/doi/abs/10.1137/1.9780898718003>, <https://arxiv.org/abs/https://epubs.siam.org/doi/pdf/10.1137/1.9780898718003>.
- [23] J. TREIBIG, G. HAGER, AND G. WELLEIN, *Likwid: A lightweight performance-oriented tool suite for x86 multicore environments*, (2010).
- [24] S. WILLIAMS, A. WATERMAN, AND D. PATTERSON, *Roofline: An Insightful Visual Performance Model for Multicore Architectures*, Commun. ACM, 52 (2009), pp. 65–76, <https://doi.org/10.1145/1498765.1498785>.

Appendix A. Algorithms.

Algorithm A.1 Construction of levels

```

1: Choose starting node(s) =  $\{n\}$ 
2:  $marked\_all = \text{false}$ 
3:  $N = n\text{rows}(\text{graph})$ 
4:  $distFromRoot[1..N] = -1$ 
5:  $curr\_children.push\_back(n)$ ;
6:  $currLvl = 0$ 
7: while  $!marked\_all$  do
8:    $marked\_all = \text{true}$ 
9:    $nxt\_children = \{\}$ 
10:  for  $i = 1 : size(curr\_children)$  do
11:    if  $distFromRoot[curr\_children[i]] == -1$  then
12:       $distFromRoot[curr\_children[i]] = currLvl$ 
13:      for  $j$  in  $graph[curr\_children[i]].children$  do
14:        if  $distFromRoot[j] == -1$  then
15:           $nxt\_children.push\_back(j)$ 
16:        end if
17:      end for
18:    end if
19:  end for
20:   $curr\_children = nxt\_children$ 
21:   $currLvl = currLvl + 1$ 
22: end while

```

Algorithm A.2 Load Balancing for two sweep, distance-2

```

1: num_sweep = 2                                % two sweep method
2: minGap = 2                                    %distance-2
3: len = num_sweep * nthread                    % constructing nthread parallel work
4: while !(exit) do
5:   T_size = update(T_ptr)                    %T_size contains non-zeros in each level group
6:   mean_r = sum(T_size[0 : num_sweep : len]) / nthreads
7:   mean_b = sum(T_size[1 : num_sweep : len]) / nthreads
8:   diff[0 : num_sweep : len] = T_size[0 : num_sweep : len] - mean_r
9:   diff[1 : num_sweep : len] = T_size[1 : num_sweep : len] - mean_b
10:  var = dot_product(diff, diff)
11:  absRankIdx = sortIdx(abs(diff)) % sortIdx returns permutation after
12:                                     % sorting from bigger to larger
13:  rankIdx = sortIdx(diff)
14:  currRank = 0, newVar = var
15:  old_T_ptr = T_ptr
16:  while newVar ≥ var do
17:    T_ptr = old_T_ptr
18:    fail = true
19:    if diff[absRankIdx[currRank]] < 0 then
20:      for el in rankIdx[(len - 1) : -1 : 0] do
21:        if (T_ptr[el + 1] - T_ptr[el]) > min_gap then
22:          acquireIdx = el
23:          fail = false
24:          break
25:        end if
26:      end for
27:      shift(T_ptr, acquireIdx, currRank) % shifts T_ptr by 1 from acquireIdx
28:                                     % to currRank if currIdx < acquireIdx else shift by -1
29:    else if (T_ptr[currRank + 1] - T_ptr[currRank]) > min_gap then
30:      giveIdx = rankIdx[0]
31:      fail = false
32:      shift(T_ptr, currRank, giveIdx)
33:    end if
34:    if !fail then
35:      newVar = calculate_variance(T_ptr) % as seen in Line 5 to Line 10
36:    end if
37:    if (currRank == (len - 1)) && (newVar ≥ var) then
38:      T_ptr = old_T_ptr
39:      exit = true
40:      break
41:    end if
42:    currRank + = 1
43:  end while
44: end while

```
